RESEARCH ARTICLE

Key Points:
- Three-dimensional global hybrid simulation of magnetotail dawn-dusk asymmetry
- Stronger Hall effect on the duskside because of the higher ion temperature, thinner current sheet, and smaller Bz there
- The asymmetry of the current sheet properties is controlled by transportations associated with the Hall effect

Hall effect control of magnetotail dawn-dusk asymmetry: A three-dimensional global hybrid simulation

San Lu[1] (iD), Y. Lin[2] (iD), V. Angelopoulos[1], A. V. Artemyev[1] (iD), P. L. Pritchett[3] (iD), Quanming Lu[4] (iD), and X. Y. Wang[2] (iD)

[1]Department of Earth, Planetary, and Space Sciences, and Institute of Geophysics and Planetary Physics, University of California, Los Angeles, California, USA, [2]Department of Physics, Auburn University, Auburn, Alabama, USA, [3]Department of Physics and Astronomy, University of California, Los Angeles, California, USA, [4]CAS Key Laboratory of Geospace Environment, Department of Geophysics and Planetary Sciences, University of Science and Technology of China, Hefei, China

Abstract Magnetotail reconnection and related phenomena (e.g., flux ropes, dipolarizing flux bundles, flow bursts, and particle injections) occur more frequently on the duskside than on the dawnside. Because this asymmetry can directly result in dawn-dusk asymmetric space weather effects, uncovering its physical origin is important for better understanding, modeling, and prediction of the space weather phenomena. However, the cause of this pervasive asymmetry is unclear. Using three-dimensional global hybrid simulations, we demonstrate that the Hall physics in the magnetotail current sheet is responsible for the asymmetry. The current sheet thins progressively under enhanced global convection; when its thickness reaches ion kinetic scales, some ions are decoupled from the magnetized electrons (the Hall effect). The resultant Hall electric field E_z is directed toward the neutral plane. The Hall effect is stronger (grows faster) on the duskside; i.e., more ions become unmagnetized there and do not comove with the magnetized dawnward $E_z \times B_x$ drifting electrons, thus creating a larger additional cross-tail current intensity j_y (in addition to the diamagnetic current) on the duskside, compared to the dawnside. The stronger Hall effect strength on the duskside is controlled by the higher ion temperature, thinner current sheet, and smaller normal magnetic field B_z there. These asymmetric current sheet properties are in turn controlled by two competing processes that correspond to the Hall effect: (1) the dawnward $E \times B$ drift of the magnetic flux and magnetized ions and electrons and (2) the transient motion of the unmagnetized ions which do not execute $E \times B$ drift.

1. Introduction

A fundamental property of the magnetotail is the dawn-dusk asymmetry of its plasma parameters and magnetic field distributions (see review by *Walsh et al.* [2014], and references therein). The most thoroughly reported asymmetry is of dynamical (transient) processes, such as flux ropes, traveling compression regions, and flow bursts, which occur predominantly in the dusk flank. A pronounced duskside preference for flux rope and traveling compression region occurrence (36 events on dawnside and 88 events on duskside) was shown in the Cluster observational statistical study by *Slavin et al.* [2005]. In the Time History of Events and Macroscale Interactions during Substorms (THEMIS) survey of flux ropes and traveling compression regions by *Imber et al.* [2011], 81% of flux ropes and traveling compression regions were observed in the dusk sector. A similar dawn-dusk asymmetry in high-speed flow occurrence has also been observed. Such an asymmetric distribution of both tailward and earthward flow bursts in the -10 R_E to -50 R_E region was reported by *Nagai and Machida* [1998] using Geotail observations. *Raj et al.* [2002] performed a statistical study using Wind data and found that 41 of 51 bulk flow events occurred on the duskside. In THEMIS statistics, similar dawn-dusk asymmetric distributions have also been found in dipolarization fronts (dipolarizing flux bundles) [*Liu et al.*, 2013] and energetic particle injection events [*Gabrielse et al.*, 2014]. The underlying common driver of these observed dawn-dusk asymmetries is the preferential occurrence of reconnection in the dusk rather than the dawn sector. A duskside reconnection event preference has been found using Geotail [*Nagai et al.*, 1998, 2013; *Machida et al.*, 1999; *Asano et al.*, 2004; *Genestreti et al.*, 2014] and Cluster [*Eastwood et al.*, 2010; *Genestreti et al.*, 2014] data.

Reconnection and related phenomena have decisive impact on global magnetospheric activities since magnetotail reconnection is widely believed to trigger substorm onset [*Baker et al.*, 1996; *Angelopoulos et al.*, 2008].

The aforementioned magnetotail dawn-dusk asymmetry can thus directly result in dawn-dusk asymmetric space weather effects. For example, previous studies have shown asymmetries in the average substorm onset location, with the most likely onset location shifted duskward to 23:00 magnetic local time [e.g., *Frey and Mende*, 2006, and references therein]. Uncovering the physical origin of this asymmetry in the magnetotail is important for better understanding, modeling, and prediction of space weather phenomena.

Recent global magnetohydrodynamic (MHD) simulations by *Lotko et al.* [2014] suggest that the asymmetry of magnetotail reconnection could be caused by the nonuniform spatial distribution (meridional gradient) of the ionospheric Hall conductance, which controls magnetosphere-ionosphere interactions through the Cowling effect. On the other hand, magnetotail dawn-dusk asymmetry has also been found to exist in a three-dimensional (3-D) global hybrid model of the magnetosphere [*Lin et al.*, 2014] even with uniform ionospheric conductance. *Lin et al.* [2014] suggested that the Hall electric field E_z, which develops because of the separation of ion and electron motion in the current sheet and thus leads to the electron and ion dawnward $E_z \times B_x$ drift, reduces the plasma content of flux tubes at dusk and results in more favorable conditions for reconnection in the dusk plasma sheet. Because the primary mechanism for triggering magnetotail reconnection is likely kinetic instabilities in the current sheet, which operate at scales on the order of a few ion gyroradii or ion inertial lengths, the Hall path to asymmetry during current sheet thinning by external forcing could precede the asymmetries imposed by ionospheric conductivity gradients.

Further analysis is required, however, to illustrate how the Hall effect generates the magnetotail dawn-dusk asymmetry. Some key questions need to be addressed: given that the Hall effect is caused by ion demagnetization, what percentage of ions are still magnetized and so can experience the $E \times B$ drift and generate a collective effect? What is the net drift in the plasma sheet when this additional drift motion is combined with other drift (e.g., diamagnetic drift) contributions? What are the magnetic field signatures (e.g., normal magnetic field B_z) associated with this mechanism, and how does the Hall effect affect the current sheet properties (e.g., cross-tail current intensity, plasma density, and current sheet thickness)? What causes the dawn-dusk asymmetric strength of the Hall effect, and how does the asymmetry progress in time? To thoroughly answer these questions, we further investigate the physical mechanism behind the Hall effect path to magnetotail dawn-dusk asymmetry. The paper is organized as follows: the 3-D global hybrid simulation model is described in section 2. The simulation results are presented in section 3. Section 4 contains the summary and discussion.

2. Simulation Model

We use the three-dimensional (3-D) global hybrid simulation model described in detail in our previous studies [e.g., *Lin et al.*, 2014; *Lu et al.*, 2015a, 2015b]. Ions are treated as particles and electrons are considered as a massless fluid. The simulation is carried out in a cubic box in the GSM coordinate system (GSM coordinates are used throughout this study). The simulation domain is from $-60\,R_E$ to $20\,R_E$ in the x direction and $-30\,R_E$ to $30\,R_E$ in the y and z directions. We use nonuniform Cartesian grids with a high resolution of $\Delta x = \Delta y = \Delta z = 0.15\,R_E$ in the near-tail region of primary interest. A total of $N_x \times N_y \times N_z = 373 \times 217 \times 217$ grids and about 3×10^9 particles are employed. The main time step for particle advancement is $dt = 0.05\ \Omega_i^{-1}$ (Ω_i based on the interplanetary magnetic field (IMF), B_{IMF}). Electromagnetic and flow fields are updated with subcycling time steps. Ten subcycling time steps are used for each main step, so the subcycling time step is $\delta t = 0.005\ \Omega_i^{-1}$. In addition to the ion particles, a cold, incompressible ion fluid is imposed in the inner magnetosphere with $r < 6\,R_E$. The subcycling time scheme and the cold ion approximation in the inner magnetosphere are enormously economical with computational resources [*Swift*, 1996]. The initial condition is a dipole geomagnetic field at $x < 15\,R_E$ (plus an image dipole) and a uniform solar wind with a southward IMF at $x > 15\,R_E$. The solar wind flows from the dayside boundary $x = 20\,R_E$ with a speed $V_{\mathrm{SW}} = -700\,\mathrm{km/s}$ along the $-x$ direction, carrying the steady IMF $B_{\mathrm{IMF}} = (0,\ 0,\ -10\,\mathrm{nT})$. The solar wind ion number density $n_{\mathrm{SW}} = 6\,\mathrm{cm}^{-3}$ and the temperature $T_{i\mathrm{SW}} = 10\,\mathrm{eV}$. The dayside boundary $x = 20\,R_E$ is a fixed boundary; the other five boundaries are open. At the inner boundary $r = 3.5\,R_E$, particles are reflected, and a magnetospheric-ionospheric electrostatic coupling model is employed [*Raeder et al.*, 1995; *Hu et al.*, 2007; *Lin et al.*, 2014]. A uniform ionospheric Pedersen conductance $\Sigma_P = 5\,\mathrm{S}$ is adopted; the Hall conductance Σ_H is assumed to be zero.
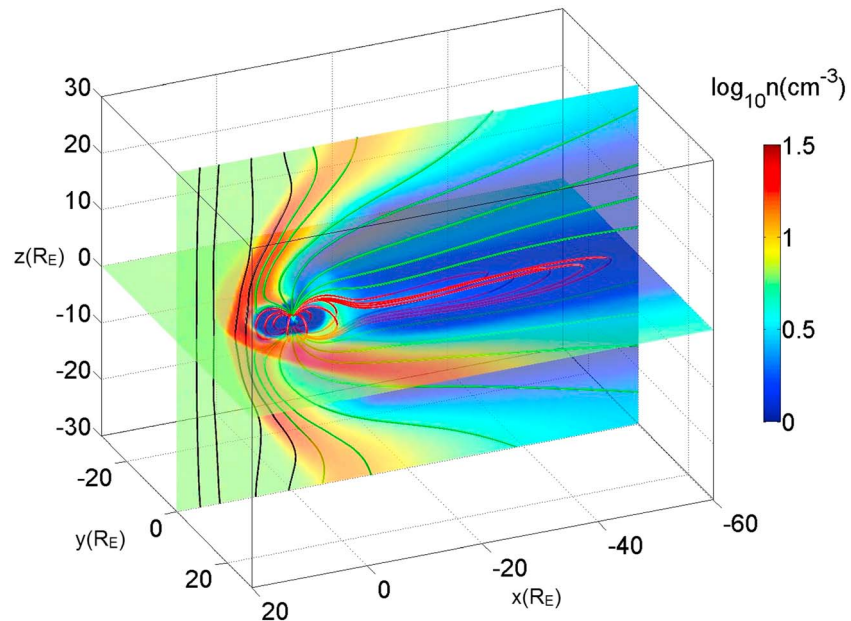
Figure 1. Overview of the 3-D global hybrid simulation. Magnetic field lines in the 3-D perspective and contours of the ion density n (cm^{-3}) in the equatorial ($z = 0$) and noon-midnight meridian ($y = 0$) planes at $t = 1430$ s. The black field lines represent the southward IMF in the solar wind and magnetosheath, the red field lines represent the closed geomagnetic field, and the green field lines represent the semiclosed geomagnetic field.

3. Simulation Results

In the 3-D global hybrid simulation, the magnetosphere is formed self-consistently by interaction between the solar wind and the geomagnetic field. At about $t = 1430$ s, well-developed bow shock, magnetosheath, and magnetosphere configurations are obtained. Figure 1 shows an overview of the hybrid simulation at that time. Southward magnetosheath field lines are reconnected with the northward geomagnetic field at the dayside magnetopause. Solar wind plasma, energy, and magnetic flux thus penetrate the magnetopause and are transported tailward by magnetospheric convection, which results in a long (in the x direction), thin current sheet in the magnetotail. As magnetic flux and energy accumulate in the magnetotail, the current sheet continues to thin until it reaches the order of the ion kinetic scale (ion inertial length or ion gyroradius).

In the ion kinetic-scale thin current sheet, ions are categorized into two classes, adiabatic/magnetized and quasi-adiabatic/unmagnetized, by different trajectories [e.g., *Sonnerup*, 1971; *Büchner and Zelenyi*, 1989; *Zhou et al.*, 2009]. The unmagnetized ions are decoupled from the magnetic field lines, whereas the electrons are frozen-in. The decoupling of ions from electrons, namely, the Hall effect, is usually characterized by the generation of a bipolar Hall electric field directed toward the neutral plane as shown in Figures 2a and 2i, for the dawn and dusk sectors, respectively. The Hall electric field E_z is distributed within the ion kinetic scale of the thin current sheet; it is stronger on the duskside (about 4 mV/m) and weaker on the dawnside (about 2 mV/m). This field can cause an $E \times B$ drift $V_{E \times B} = E \times B/B^2$ from dusk to dawn. In the y direction, $V_{E \times B} = (E_z B_x - E_x B_z)/B^2$. In a thin current sheet, E_x and B_z (and B_y) are much smaller than E_z and B_x, respectively; therefore, $V_{E \times B} \approx E_z/B_x$. However, we should note that both B_x and E_z reverse across the neutral plane, $B_x = 0$. Therefore, the $E \times B$ drift near $B_x = 0$ is mainly contributed by E_x instead of E_z [*Zelenyi et al.*, 2010]. In the thin current sheet with small external guide field ($B_y \ll B_x$; this condition is satisfied in our simulation because of the zero IMF B_y) and small parallel electric field ($E_{\parallel} \sim 0$; this condition is also satisfied before magnetotail reconnection occurs in our simulation), the electric field E_x component is related to E_z components: $E_x \approx -E_z B_z/B_x$. By substituting this relation to $V_{E \times B} = (E_z B_x - E_x B_z)/(B_x^2 + B_z^2)$, we obtain $V_{E \times B} \approx E_z/B_x$, which only contains E_z and B_x. The ratio E_z/B_x has a finite value at the neutral plane (both $E_z \sim z$ and $B_x \sim z$ near $z \sim 0$). Therefore, the expression $V_{E \times B} \approx E_z/B_x$ is still valid even near the neutral sheet, and thus, we consider E_z as the main contributor to the $E \times B$ drift [*Schindler and Birn*, 2002; *Schindler et al.*, 2012].
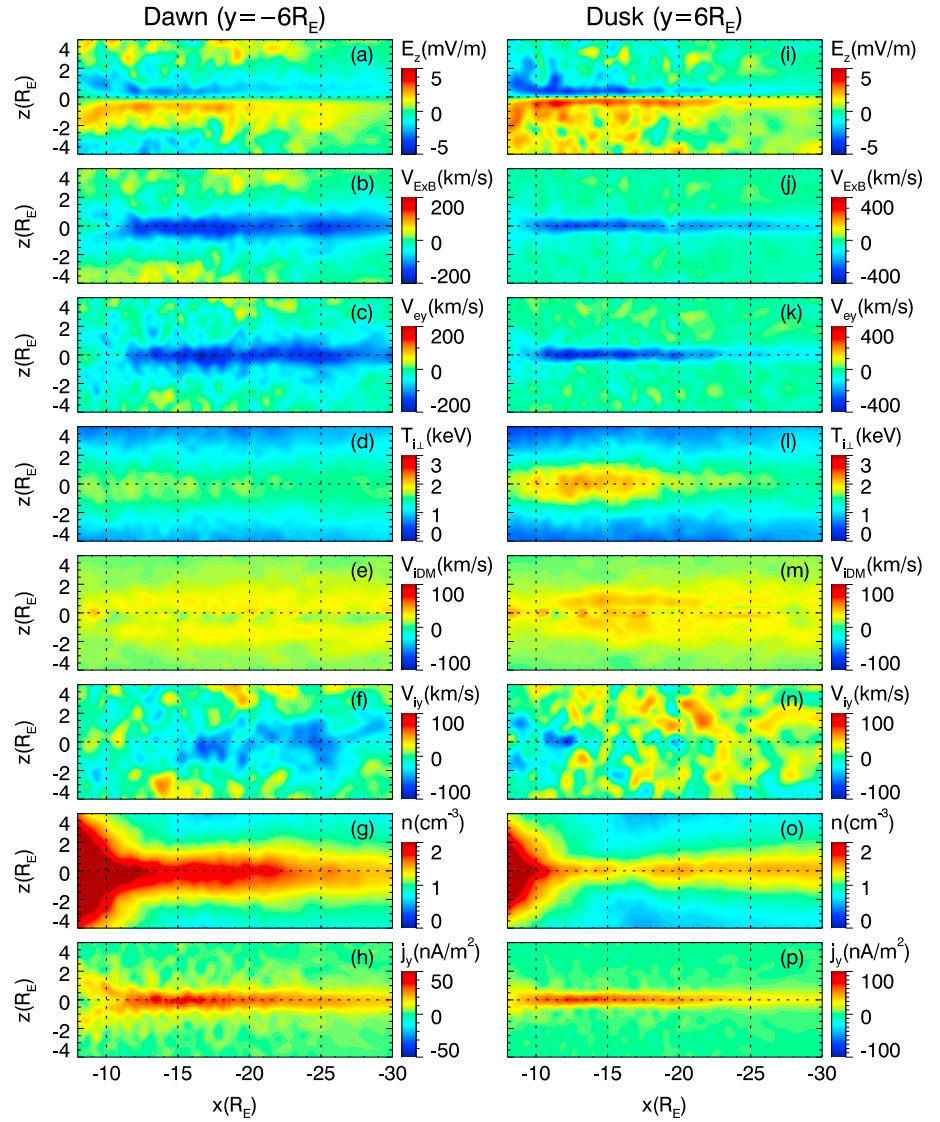
Figure 2. Contours of (a and i) E_z (mV/m), (b and j) $E \times B$ drift velocity $V_{E \times B} = (E_z B_x - E_x B_z)/B^2$ (km/s), (c and k) electron bulk velocity V_{ey} (km/s), (d and l) ion perpendicular temperature $T_{i\perp}$ (keV), (e and m) ion diamagnetic drift velocity $V_{iDM} = -[B_x \nabla_z(nT_{i\perp}) - B_z \nabla_x(nT_{i\perp})]/(enB^2)$ (km/s), (f and n) ion bulk velocity V_{iy} (km/s), (g and o) number density n (cm^{-3}), and (h and p) cross-tail current density j_y (nA/m^2) in the dawnside ($y = -6 \, R_E$) and duskside ($y = 6 \, R_E$) (x, z) planes at $t = 1430$ s.

Because E_z is stronger on the duskside, the $E \times B$ drift is also stronger there (about 300 km/s) and weaker (about 150 km/s) on the dawnside (see Figures 2b and 2j). The electrons in the thin current sheet are almost all magnetized, and their motion is dominated by the $E \times B$ drift. The electron flow velocity in the y direction can be written as $V_{ey} = V_{eDM} + V_{E \times B}$, where electron diamagnetic drift V_{eDM} is negligible because of the low electron temperature. Therefore,

$$V_{ey} = V_{E \times B}, \tag{1}$$

which is demonstrated in Figures 2b, 2c, 2j, and 2k.

The $E \times B$ drift discussed above causes a net momentum change in addition to the equilibrium diamagnetic drift in the current sheet. As a result, the overall ion flow is more complicated because it is a combination of ion diamagnetic drift $V_{iDM} = B \times \nabla(nT_{i\perp})/(enB^2)$ (in the y direction, $V_{iDM} = -[B_x \nabla_z(nT_{i\perp}) - B_z \nabla_x(nT_{i\perp})]/(enB^2) \approx -B_x \nabla_z(nT_{i\perp})/(enB^2))$ of all the ions and $E \times B$ drift of the magnetized ions. Unmagnetized ions move

along transient (Speiser) trajectories, so they do not have chance to make a closed orbit within current sheet [e.g., *Büchner and Zelenyi*, 1989]. As a result, these particles do not follow the guiding center $E \times B$ drift but contribute to the V_{iDM} drift [e.g., *Sitnov et al.*, 2000; *Zelenyi et al.*, 2000]. Therefore, the total ion flow velocity is

$$V_{iy} = V_{iDM} + \alpha_i V_{E \times B}, \tag{2}$$

where α_i (<1) is the fraction of the magnetized ions. The ion perpendicular temperature $T_{i\perp}$ is higher on the duskside in the thin current sheet (see Figures 2d and 2l). Such an asymmetry is consistent with previous observations and modeling [*Spence and Kivelson*, 1990; *Wang et al.*, 2006; *Guild et al.*, 2008; *Keesee et al.*, 2011; *Vasko et al.*, 2015]. The higher $T_{i\perp}$ and thinner current sheet on the duskside give an ion diamagnetic drift speed that is higher (about 50 km/s) on the duskside and lower (about 25 km/s) on the dawnside (see Figures 2e and 2m). Figures 2f and 2n present the ion flow velocity in the y direction on the duskside and dawnside. On the duskside, the ion flow velocity is about 10 km/s. Given, from above, that $V_{iDM} = 50$ km/s and $V_{E \times B} = -300$ km/s on the duskside, $\alpha_i = 0.13$ can be obtained using equation (2). On the dawnside, $V_{iy} = -50$ km/s, $V_{iDM} = 25$ km/s, and $V_{E \times B} = -150$ km/s, so $\alpha_i = 0.5$. Therefore, we infer that more ions are unmagnetized on the duskside ($1 - \alpha_i = 87\%$) than on the dawnside ($1 - \alpha_i = 50\%$). The plasma density is also asymmetric, higher on the dawnside, and lower on the duskside (see Figures 2g and 2o). Combining this plasma density asymmetry with the higher ion perpendicular temperature on the duskside than on the dawnside, the pressure ($P_{i\perp} = nT_{i\perp}$) is balanced between the dawnside and duskside.

The cross-tail current density can be written as

$$j_y = en(V_{iy} - V_{ey}) = en[V_{iDM} + (1 - \alpha_i)|V_{E \times B}|]. \tag{3}$$

All the properties (larger V_{iDM}, smaller α_i, and larger $|V_{E \times B}|$) on the duskside lead to a much more intense cross-tail current density on the duskside, as shown in Figures 2h and 2p. By comparing the electron and ion flow velocities in the y direction, one can see that the cross-tail current is predominately carried by the electrons in the thin current sheet, which is generated by the $E \times B$ drift due to the Hall electric field. The first term on the right-hand side of equation (3) is the diamagnetic current (V_{eDM} neglected), and the second term is the additional current introduced by the Hall effect. In the thin current sheet, especially on the duskside, the cross-tail current density j_y is predominantly contributed by the Hall effect term.

To further demonstrate the current sheet properties and their dawn-dusk asymmetry, Figure 3 shows the profiles of current sheet properties along the z direction averaged from $x = -20\ R_E$ to $-15\ R_E$ on the dawnside ($y = -6\ R_E$) and duskside ($y = 6\ R_E$). The j_y peak is 34.2 nA/m^2 on the dawnside and 67.2 nA/m^2 on the duskside. The j_y profiles show a typical "embedded thin current sheet" [*Runov et al.*, 2006; *Sitnov et al.*, 2006; *Petrukovich et al.*, 2011], i.e., a thin current sheet embedded within a thicker background plasma sheet. We fit the j_y profiles with a simple embedded thin current sheet model, $j_y = j_0 \text{sech}^2(z/L_0) + j \text{sech}^2(z/L)$, where the first term on the left-hand side represents the thick background plasma sheet with small current density j_0 and large thickness L_0, and the second term represents the embedded thin current sheet with intense current density j and small thickness L. The fitted current sheet half-thickness is $L = 0.6\ R_E$ on the dawnside and $L = 0.33\ R_E$ on the duskside. Note that because of the limited computer resources, we use an artificial solar wind ion inertial length $d_{iSW} = 0.1\ R_E$ (6.85 times larger than actual value) in the 3-D global hybrid simulations [*Lin et al.*, 2014; *Lu et al.*, 2015a, 2015b]. As shown in Figures 3c and 3h, the number density in the magnetotail is 1.81 cm^{-3} = 0.3 n_{SW} (1.4 cm^{-3} = 0.23 n_{SW}) on the dawnside (duskside), so the ion inertial length in the magnetotail is about $d_i = 0.18\ R_E$ ($d_i = 0.21\ R_E$) on the dawnside (duskside). Therefore, the above current sheet thicknesses actually correspond to 3.3 d_i and 1.6 d_i on the dawnside and duskside, respectively, for realistic magnetotail parameters. The ion density and temperature are all peaked at the center of the thin current sheet (see Figures 3b, 3c, 3g, and 3h). On the duskside (dawnside), the ion density is lower (higher) and temperature is higher (lower). The B_x profiles (see Figures 3d and 3i) also show that the thin current sheet (larger gradient at the center) is embedded in the thick plasma sheet (smaller gradient in the outer region). The ambient magnetic field magnitude B_0 of the thin current sheet is obtained by integrating j_y over $0 < z - z_0 < L$, where z_0 is the location of the neutral plane. Figures 3e and 3j show that the normal magnetic field B_z in the thin current sheet is also dawn-dusk asymmetric, much smaller on the duskside. The smaller B_z on the duskside, along with the thinner current sheet and higher ion temperature there, make more ions become unmagnetized, further separating the ion motion from the magnetized electron motion, which results in a stronger Hall effect on the duskside.
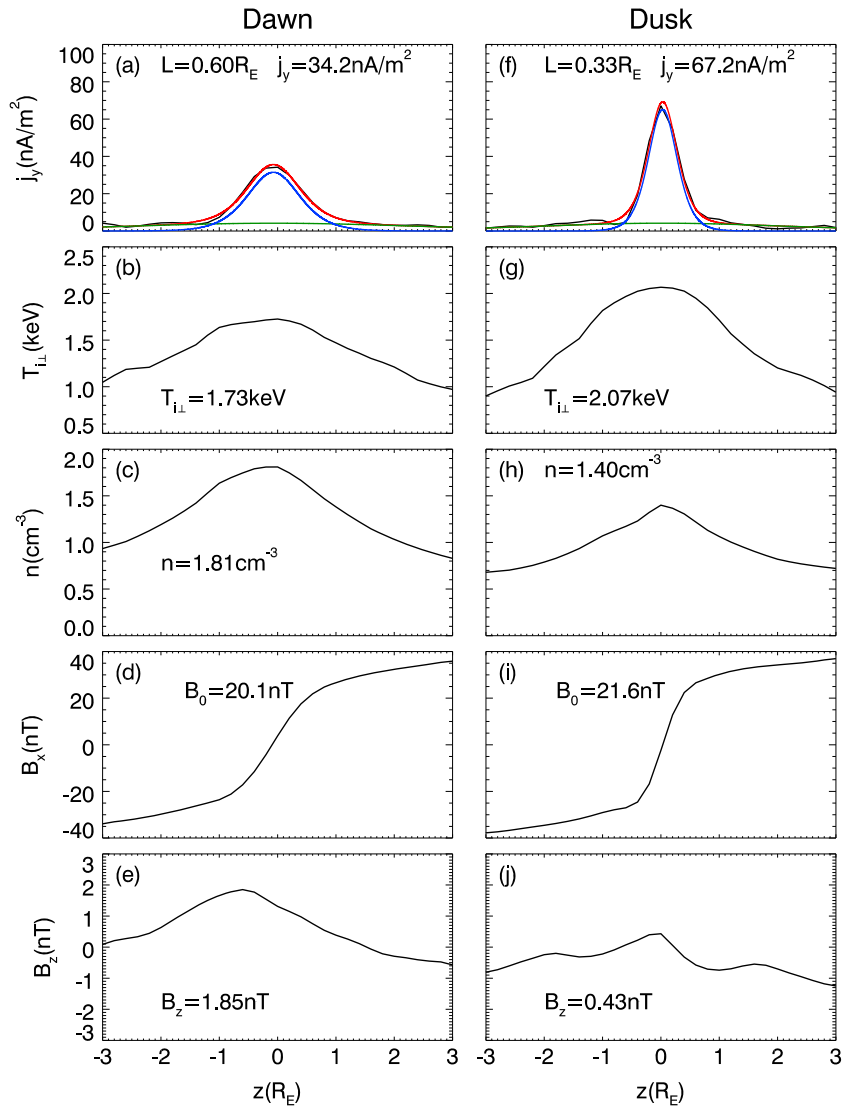
Figure 3. Profiles of (a and f) cross-tail current density j_y (nA/m^2), (b and g) perpendicular temperature $T_{i\perp}$ (keV), (c and h) number density n (cm^{-3}), and magnetic field components (d and i) B_0 (nT) and (e and j) B_z (nT) along the z direction averaged from $x = -20$ R_E to -15 R_E. The current density j_y is fitted with the embedded current sheet model, $j_y = j_0 \text{sech}^2(z/L_0) + j \text{sech}^2(z/L)$. The blue curve denotes the embedded thin current sheet, the green curve denotes the thick plasma sheet, and the red curve denotes their sum.

Figures 4–6 show the evolution of the ion perpendicular temperature, Hall electric field, and cross-tail current density, respectively, to demonstrate how the dawn-dusk asymmetry evolves. From $t = 1072$ s to 1430 s, the ion perpendicular temperature, as shown in Figure 4, increases from about 1 keV to about 2.5 keV at -20 $R_E < x < -10$ R_E on the duskside ($y = 6$ R_E), while it increases much less on the dawnside ($y = -6$ R_E). Ions with higher temperature have larger duskward gradient/curvature drift velocity; therefore, hotter ions tend to be transported to the duskside, which leads to the fast increase of $T_{i\perp}$ on the duskside. The Hall electric field E_z also grows much faster on the duskside than the dawnside (see Figure 5): at $t = 1072$ s, its magnitude is almost similar on the dawnside and duskside, about 1.5 mV/m, but at $t = 1430$ s, it is much stronger on the duskside, indicating a stronger Hall effect there. We suggest that this is related to the higher ion temperature, thinner current sheet, and smaller B_z there; all of which result in a higher fraction of the ions being unmagnetized and contributing to the ion motion becoming separated from that of the electrons. The faster growing Hall effect on the duskside leads to a faster growing cross-tail current density there compared to the dawnside, as shown in Figure 6.
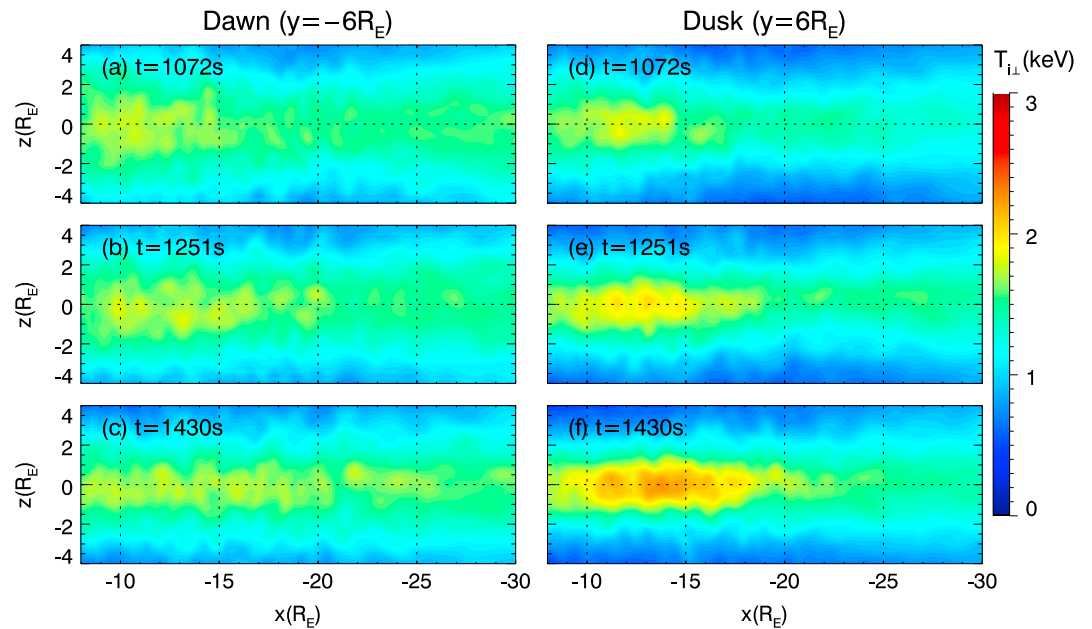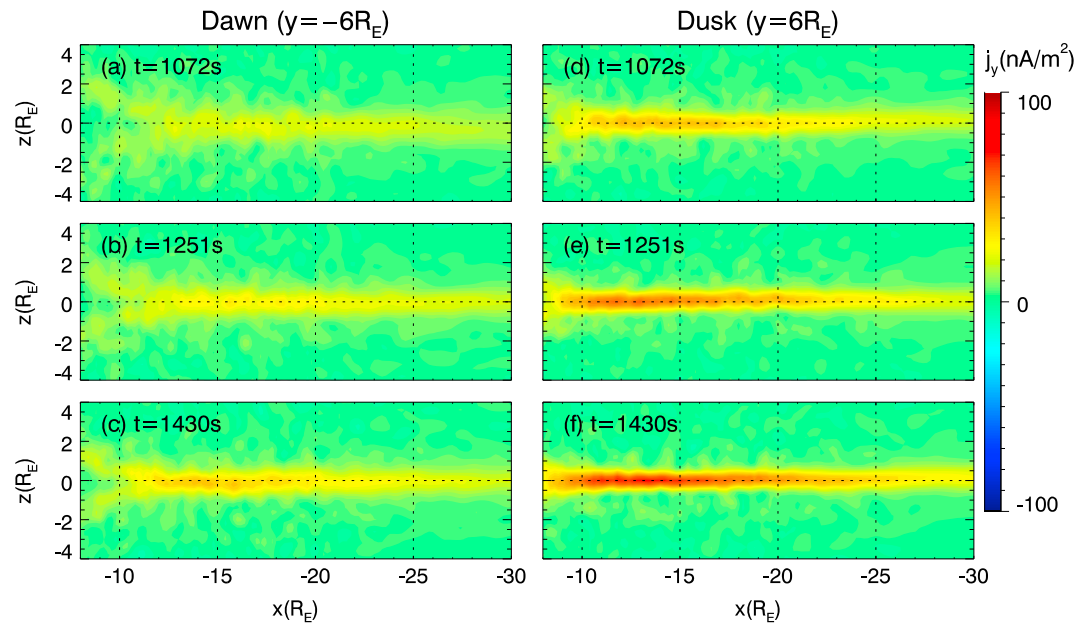
Figure 4. Ion perpendicular temperature $T_{i\perp}$ (keV) at (a and d) $t = 1072$ s, (b and e) 1251 s, and (c and f) 1430 s in the dawnside ($y = -6\,R_E$) and duskside ($y = 6\,R_E$) (x, z) planes.

Figure 7 shows the complete temporal evolution of characteristic parameters of the thin current sheet on the dawn and dusk flanks. The ion perpendicular temperature $T_{i\perp}$ on the dawnside is almost unchanged, from 1.6 keV at $t = 785$ s to 1.7 keV at $t = 1430$ s, while $T_{i\perp}$ increases more significantly on the duskside, from 1.2 keV at $t = 785$ s to 2.1 keV at $t = 1430$ s (see Figure 7a). During the same time, the density shows an opposite trend (see Figure 7b): it increases on the dawnside (from 1.4 cm^{-3} at $t = 785$ s to 1.7 cm^{-3} at $t = 1430$ s) and decreases on the duskside (from 1.7 cm^{-3} at $t = 785$ s to 1.4 cm^{-3} at $t = 1430$ s). The ion perpendicular pressure $P_{i\perp} = nT_{i\perp}$ increases and is balanced between the dawnside and duskside (see Figure 7c), suggesting
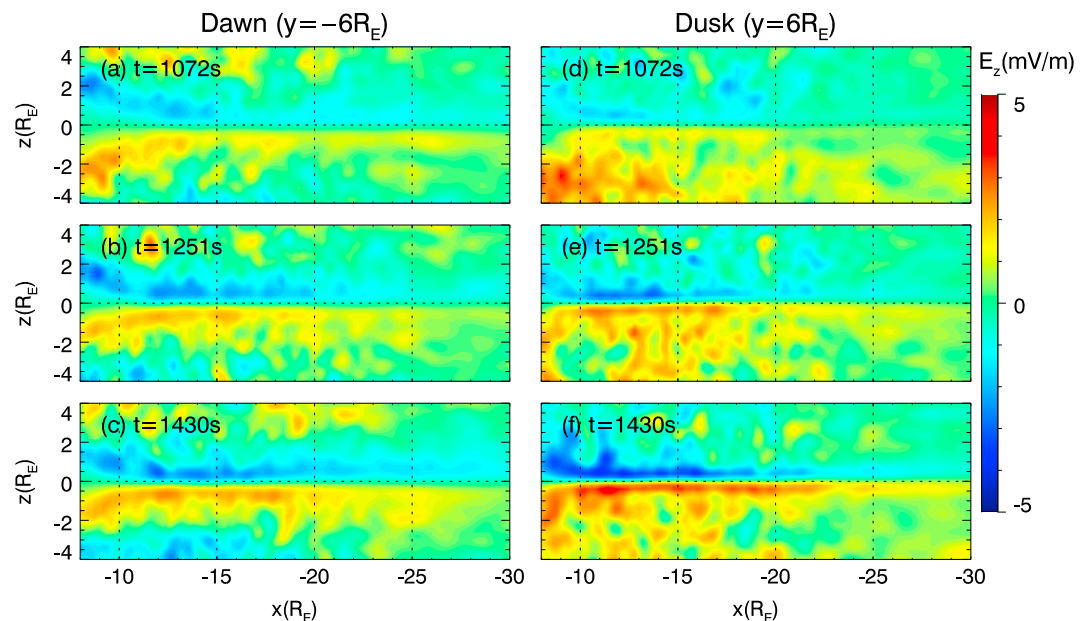

Figure 5. Hall electric field E_z (mV/m) at (a and d) $t = 1072$ s, (b and e) 1251 s, and (c and f) 1430 s in the dawnside ($y = -6\,R_E$) and duskside ($y = 6\,R_E$) (x, z) planes.

Figure 6. Cross-tail current density j_y (nA/m^2) at (a and d) $t = 1072$ s, (b and e) 1251 s, and (c and f) 1430 s in the dawnside ($y = -6\ R_E$) and duskside ($y = 6\ R_E$) (x, z) planes.

that the lobe magnetic field $B_L \approx (2\mu_0 p_{i\perp})^{1/2}$ is dawn-dusk symmetric. Therefore, the total cross-tail linear current density $\sigma_y = \int j_y dz = \mu_0 B_L$ is dawn-dusk symmetric, although j_y is asymmetrically distributed across the plasma sheet-current sheet, having a stronger peak within the embedded ion-scale, thin current sheet on the duskside.

The magnetic flux is frozen-in with the magnetized plasma and also transported from the duskside to the dawnside by the $E \times B$ drift, which causes a smaller B_z on the duskside. Therefore, although at an earlier time, $t = 785$ s, the normal magnetic field B_z magnitude is almost symmetric on the dawnside and duskside, as time
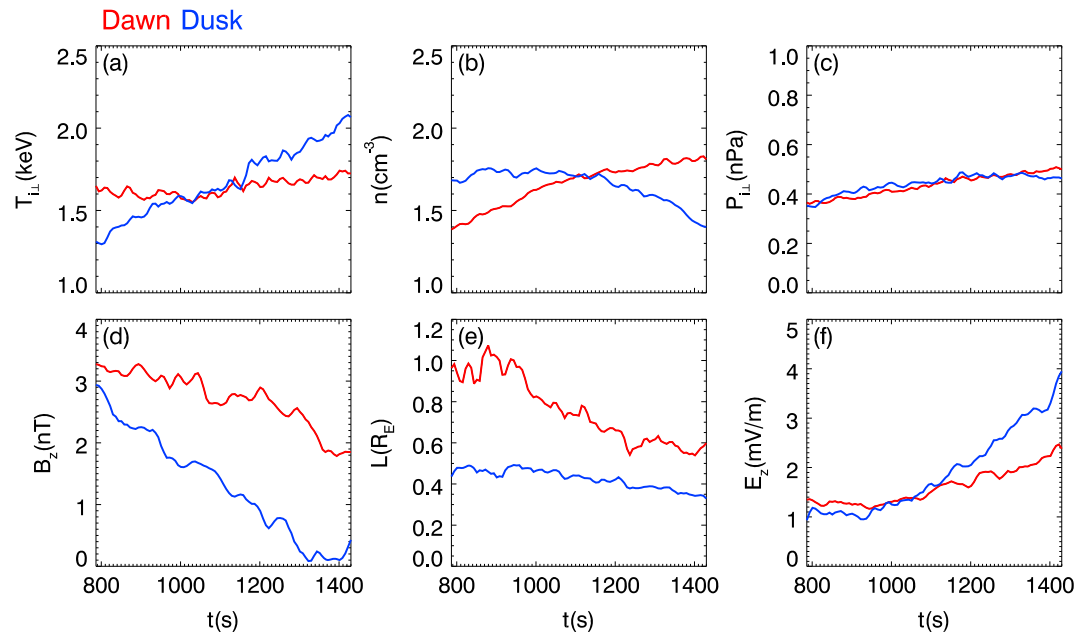
Figure 7. Evolution of (a) ion perpendicular temperature $T_{i\perp}$ (keV), (b) number density n (cm^{-3}), (c) ion perpendicular pressure $P_{i\perp}$ (nPa), (d) normal magnetic field B_z (nT) in the current sheet, (e) current sheet half-thickness L (R_E), and (f) Hall electric field magnitude E_z (mV/m) on the dawnside ($y = -6\ R_E$) and duskside ($y = 6\ R_E$) averaged from $x = -20\ R_E$ to $-15\ R_E$.
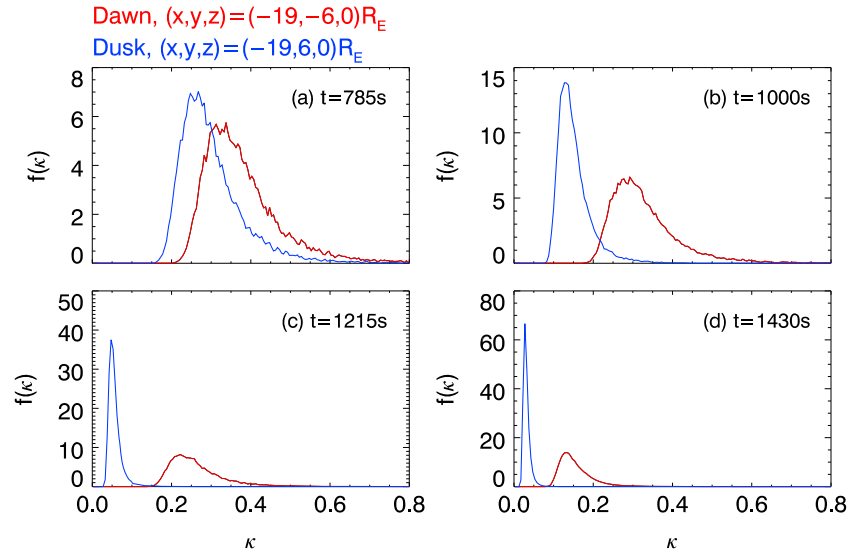
Figure 8. Distribution function of parameter κ at (a) $t = 785$ s, (b) 1000 s, (c) 1215 s, and (d) 1430 s on the dawnside (at $(x, y, z) = (-19, -6, 0)\ R_E$) and duskside (at $(x, y, z) = (-19, 6, 0)\ R_E$). The distribution function satisfies $\int f(\kappa)d\kappa = 1$.

goes on the $E \times B$ drift grows stronger, and the asymmetry of B_z intensifies (see Figure 7d). Next, we examine if the B_z asymmetry can be caused by the dawnward transportation of $E \times B$ drift: the transported normal magnetic flux per meter in the x direction from dusk to dawn by $E \times B$ drift is $\Delta \Phi = B_z V_{E \times B} \Delta t$. From $t = 785$ s to 1430 s, $B_z \approx 2$ nT, $V_{E \times B} \approx 100$ km/s, and $\Delta t = 645$ s, so $\Delta \Phi \approx 0.129$ Wb/m. The dawn-dusk difference of the normal magnetic flux per meter in the x direction is $\Delta \Phi^* = \Delta B_z L_y$, where ΔB_z is the B_z difference between the dawnside and duskside, and $L_y \approx 15\ R_E \approx 9.5 \times 10^7$ m is the length of the magnetotail dawn (dusk) flank. At $t = 1430$ s, $\Delta B_z = 1.85$ nT–0.43 nT = 1.42 nT, so we have $\Delta \Phi^* \approx 0.135$ Wb/m. We thus get $\Delta \Phi \approx \Delta \Phi^*$, which supports the idea that the dawn-dusk difference of the normal magnetic flux is caused by the transportation of flux by the $E \times B$ drift. The duskside current sheet with having plasma and magnetic flux is more easily to undergo further thinning than the dawnside. Therefore, the current sheet is also thinner on the duskside (see Figure 7e). The above asymmetric evolution of the thin current sheet is likely controlled by the different motions of a significant thermal/suprathermal portion of the ions that is unmagnetized compared to the magnetized cold ions and electrons. This behavior is the origin of the Hall effect as indicated by the Hall electric field E_z. As shown in Figure 7f, E_z is stronger and grows faster on the duskside compared to the dawnside.

The strength of the Hall effect, or the fraction of the unmagnetized and magnetized ions, is in turn determined by current sheet properties like ion temperature, current sheet thickness L, and normal magnetic field B_z. Our previous estimation of α_i (the fraction of the magnetized ions) based on Figure 2 and equation (2) roughly shows that more ions are unmagnetized on the duskside, which means that the Hall effect is stronger on the duskside. Here we further prove this using the ions' κ parameters [see, e.g., *Büchner and Zelenyi*, 1989]. In the thin current sheet, each ion has a κ parameter, defined as the square root of the magnetic field's curvature radius divided by the ion's Larmor radius (both calculated in the neutral plane, $B_x = 0$),

$$\kappa = \frac{B_z}{B_0} \sqrt{\frac{L}{\rho_0}}, \tag{4}$$

where B_z is the normal magnetic field in the thin current sheet, B_0 is the ambient magnetic field of the thin current sheet, L is the current sheet half-thickness, and ρ_0 is the ion's Larmor radius ($\rho_0 = \frac{\sqrt{2E/m_i}}{\Omega_0}$ and $\Omega_0 = \frac{eB_0}{m_i}$). Note that the κ parameter is controlled by the ion energy (through ρ_0), current sheet thickness L, and B_z magnitude. Particles are totally magnetized when their magnetic moments are well conserved, which is satisfied for the particles with $\kappa > 2$ [*Birmingham*, 1984]. Ions with $\kappa \sim 1$ have very chaotic trajectories [*Büchner and Zelenyi*, 1986; *Delcourt and Belmont*, 1998]. Separation of the magnetized electron motion and the chaotic ion motion results in the generation of the Hall electric field, but the chaotic ions being trapped within the current sheet are drifting in this electric field and cannot participate in current density
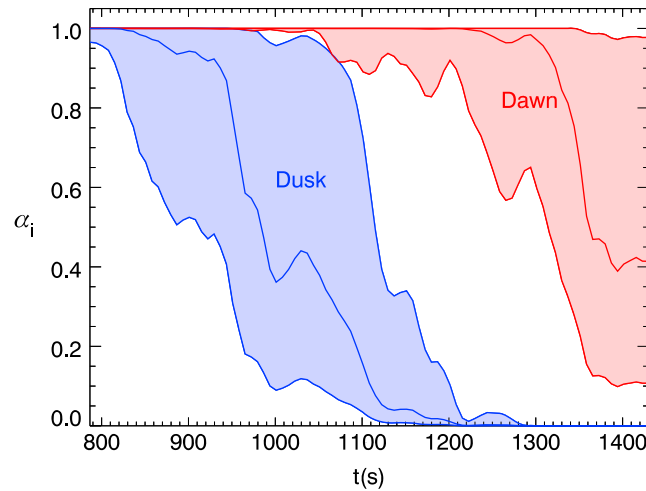
Figure 9. Evolution of α_i, the fraction of the magnetized ions when $\kappa_c = 0.1$–0.2 on the dawnside (at $(x, y, z) = (-19, -6, 0)\ R_E$) and duskside (at $(x, y, z) = (-19, 6, 0)\ R_E$). The upper, middle, and lower curves correspond to the $\kappa_c = 0.1$, 0.15, and 0.2, respectively.

generation (do not contribute to the α_i decrease). Only ions with $\kappa < 0.1$–0.2 move along transient trajectories [*Büchner and Zelenyi*, 1989; *Burkhart et al.*, 1992], which are not closed within current sheet where the Hall electric field is localized. This (transient) ion population does not execute the $E \times B$ drift and is thus responsible for the α_i decrease. Therefore, the κ parameter determines whether an ion is fully magnetized (or chaotic) or unmagnetized (transient) by choosing a critical κ value, κ_c. If $\kappa < \kappa_c$, the ion is unmagnetized; otherwise, it is magnetized.

Figure 8 shows the distribution function of the ions expressed in units of κ on the dawnside and duskside at different times. At earlier times, for example at $t = 785$ s, the dawn-dusk asymmetry (of $T_{i\perp}$, L, and B_z) in the thin current sheet is weak, so the difference between $f(\kappa)$ on the dawnside and duskside is small, with κ predominately distributed around 0.3 on the dawnside and 0.25 on the duskside. At later times when the asymmetry of the current sheet properties becomes larger, the distributions on the dawnside and duskside are well distinguished. For example, at $t = 1430$ s, $f(\kappa)$ is peaked at about 0.15 on the dawnside and 0.025 on the duskside, which proves that more ions are unmagnetized (transient) on the duskside because of their smaller κ. Overall, κ decreases because of the thinning and stretching of the thin current sheet.

Figure 9 shows the evolution of the fraction of the magnetized (nontransient) ions (with $\kappa > \kappa_c$) $\alpha_i = N(\kappa > \kappa_c)/N$ when $\kappa_c = 0.1$–0.2 (a good critical κ value to separate the magnetized/nontransient and unmagnetized/transient ions [*Büchner and Zelenyi*, 1989; *Burkhart et al.*, 1992]). Note that the result is sensitive to the choice of κ_c, but no matter which κ_c we choose, the fraction of the magnetized ions α_i is always smaller on the duskside, which means that more ions are unmagnetized on the duskside than the dawnside. For example, as shown in Figure 9, if $\kappa_c = 0.15$, at $t = 1430$ s, $\alpha_i \approx 0$ on the duskside and about $\alpha_i \approx 0.4$ on the dawnside, which means that there is no any significant transient ion population on the duskside (only magnetized and chaotic ions trapped within the current sheet) and about 60% of the ions are magnetized (or moving along chaotic trajectories) on the dawnside. The result is consistent with our previous estimation based on equation (2). From $t = 785$ s to 1430 s, the decrease of α_i shows that more and more ions become unmagnetized during the thinning/stretching of the thin current sheet, especially on the duskside, which leads to a stronger and stronger Hall effect there.

4. Summary and Discussion

In summary, we investigated Hall effect control of dawn-dusk asymmetry in the magnetotail thin current sheet using a 3-D global hybrid simulation model under the southward IMF. The main results are given below.

1. Through magnetospheric global convection, the magnetotail current sheet thins and reaches the order of ion kinetic scale (ion inertial length or ion gyroradius).
2. In the thin current sheet, electrons are magnetized. Ions are categorized into two classes, unmagnetized and magnetized. The unmagnetized ions are decoupled from the electrons (the Hall effect), which forms a bipolar Hall electric field E_z directed toward the neutral plane.
3. The unmagnetized ions (contribute to the duskward diamagnetic drift) cannot comove with the magnetized dawnward $E_z \times B_x$ drifting electrons; therefore, a pronounced additional cross-tail current density j_y (in addition to the diamagnetic current) is formed.

4. More ions are unmagnetized (stronger Hall effect) on the duskside, generating a larger Hall electric field E_z and a larger cross-tail current density j_y there.

5. In the magnetotail thin current sheet, the normal magnetic field B_z is smaller, the current sheet is thinner, the ion perpendicular temperature is higher, and the density is lower on the duskside. On the other hand, the ion perpendicular pressure in the thin current sheet and thus the lobe magnetic field and total cross tail current are balanced between the dawnside and duskside.

6. We suggest the above asymmetric properties are controlled by two competing processes that correspond to the Hall effect: (1) the dawnward $E \times B$ drift of the magnetic flux and magnetized ions and electrons and (2) the transient motion of the unmagnetized ions which do not execute $E \times B$ drift.

7. Analysis based on the ions' κ parameters shows that the asymmetry of the Hall effect (indicated by smaller α_i and stronger E_z and j_y) on the duskside, in turn, is determined by the asymmetry of the current sheet properties. The higher ion perpendicular temperature $T_{i\perp}$, smaller current sheet thickness L, and smaller B_z on the duskside determine the stronger Hall effect there.

The idea that the Hall effect controls the magnetotail dawn-dusk asymmetry was first proposed by *Lin et al.* [2014], who attributed the asymmetry to a dawnward ion $E \times B$ drift motion in the Hall electric field, resulting in a dawn-dusk asymmetry of the plasma sheet density (higher on the dawnside and lower on the duskside). In this paper, we further investigated the Hall effect in the magnetotail thin current sheet and the role it plays in generation of the dawn-dusk asymmetry. We found that a fraction of the ions are unmagnetized, contributing to the Hall effect but do not execute $E \times B$ drift, while other ions are magnetized, which do not contribute to the Hall effect but drift from dusk to dawn by the $E \times B$ drift. Our analysis based on the ions' κ parameters showed that because the ion perpendicular temperature is higher, the current sheet is thinner, and B_z is smaller on the duskside, more ions are unmagnetized, leading to a stronger Hall effect and thus a larger cross-tail current density.

The dawn-dusk asymmetric properties of the magnetotail current sheet obtained in our hybrid simulation: (1) larger cross-tail current density j_y on the duskside, (2) lower density on the duskside, (3) higher ion perpendicular temperature, (4) smaller B_z on the duskside, and (5) thinner current sheet on the duskside, contribute to cause magnetic reconnection and related phenomena to preferentially occur on the duskside. These asymmetric properties of the magnetotail current sheet have been observed by spacecraft and are consistent with our simulation results. For example, using statistics of 70 thin current sheet crossings in the near tail by the Cluster spacecraft, *Artemyev et al.* [2011] found that on the duskside the cross-tail density is larger, the current sheet is thinner, and B_z is smaller. More recently, *Vasko et al.* [2015] performed Geotail crossing statistics and found similar dawn-dusk asymmetric thin current sheet properties in the distant tail, which showed that the dawn-dusk asymmetry is ubiquitous in the magnetotail. The ion temperature and density asymmetries were also observed by Geotail [*Wang et al.*, 2006; *Guild et al.*, 2008] and Two Wide-angle Imaging Neutral-atom Spectrometers [*Keesee et al.*, 2011], and showed that the ion temperature is higher on the duskside and the ion density is higher on the dawnside, which gives a pressure balance between the dawn and dusk flanks. We further discussed how these asymmetric current sheet properties are formed: the unmagnetized ions (usually have a higher average energy) are drifted duskward via the ion gradient/curvature drift, so that the ion temperature on the duskside is higher than that on the dawnside. On the other hand, the magnetized ions along with the electrons (almost all magnetized) and magnetic flux are transported from dusk to dawn by the $E \times B$ drift, which may be the reason for the lower density and a smaller B_z on the duskside than on the dawnside. At the same time, the duskside current sheet with less plasma and magnetic flux is more easily to get further thinning than the dawnside. Therefore, the current sheet is also thinner on the duskside. Although we attribute the density asymmetry to the dawnward transportation of the magnetized particles by the $E \times B$ drift, the reality is more complicated because the $E \times B$ drift moves the magnetized ions and electrons from dusk to dawn but leaves the unmagnetized ions behind, which is suppose to generate a charge separation. However, the system will try to maintain quasi-neutrality either by dissipating the redundant electrons on the dawnside through magnetic field lines to the ionosphere or (2) by generating an electrostatic field to move more ions (or less electrons) from the duskside to the dawnside. The dawn-dusk pressure balance can also dictate the ion density distribution given the influx of hot ions through dawn-dusk convection. A better modeling of the electrons and the ionosphere and further investigations, considering the different time scales of these processes, are needed in the future to get a more thorough understanding of the dawn-dusk plasma transportation and how the quasi-neutrality is obtained.

The Hall effect has been thoroughly studied in the context of magnetic reconnection [e.g., *Shay et al.*, 1998; *Birn et al.*, 2001; *Nagai et al.*, 2001]. The Hall effect in the thin current sheet (before reconnection) discussed in this paper is similar to the Hall effect in reconnection layer but does not require reconnection to separate ions and electrons. Rather, the thinness of the current sheet is sufficient to result in a large enough Hall electric field to impart global changes to the plasma sheet. The thin current sheet's thickness is about several ion inertial lengths, while the thickness of the reconnection layer is $\lambda_{ez} = \left[\frac{2m_e T_e}{e^2 (\partial B_x / \partial z)^2}\right]^{1/4}$ [e.g., *Biskamp and Schindler*, 1971; *Hesse et al.*, 1999], even thinner than the thin current sheet. As a result, in the reconnection layer, almost all the ions are unmagnetized and nearly all the cross-tail current is carried by the electrons [*Fujimoto*, 2006]; therefore, the reconnection layer is usually called electron diffusion region or electron current sheet. Our simulation showed that in the thinner duskside current sheet, the Hall effect is stronger than on the dawnside with the Hall electric field about 4 mV/m (on the dawnside the Hall effect is weaker and the Hall electric field is about 2 mV/m). In the even thinner electron current sheet during reconnection, the Hall effect is much stronger than that in the thin current sheet, and the Hall electric field is about 25 mV/m during magnetotail reconnection [e.g., *Borg et al.*, 2005; *Eastwood et al.*, 2010]. The Hall electric field is formed by the electron-ion charge separation and balanced by the Hall term in the generalized Ohm's law. Therefore, the Hall electric field is the electrostatic electric field due to the fact that the electron-dominated current sheet is charged [*Yoon and Lui*, 2004]. The Hall electric field E_z in the thin current sheet has been simulated with hybrid [e.g., *Hesse et al.*, 1998] and full particle [*Pritchett and Coroniti*, 1994, 1995; *Pritchett et al.*, 1996] simulations. Nevertheless, the dawn-dusk asymmetry of E_z cannot be explored easily with these local simulations.

Previous global MHD simulations suggested that the magnetotail dawn-dusk asymmetry is caused by the spatially nonuniform ionospheric conductance, which controls magnetosphere-ionosphere interactions [*Lotko et al.*, 2014]. In our global hybrid simulation, where the ionospheric conductance was uniform, the dawn-dusk asymmetry was found to be due to the Hall effect and the resultant $E \times B$ drift in the ion kinetic-scale thin current sheet. At the same time, our simulation showed that the magnetotail is globally symmetric (indicated by the symmetric lobe magnetic field B_L and the total linear cross-tail current density σ_y), which may be because of the uniform ionospheric conductance. This situation in our simulation, globally symmetric and locally asymmetric, suggests that the magnetotail asymmetry in our simulation is not originated from the external effects (e.g., global convection and ionosphere-magnetosphere interaction) but controlled by the magnetotail intrinsic evolution during the substorm growth-phase-type process. For a more thorough understanding of the physical origin of the dawn-dusk asymmetry, in the future, a nonuniform ionospheric conductance will be imposed into our global hybrid model to investigate how the two effects, ionosphere-magnetosphere interaction and Hall effect, control the magnetotail asymmetry in both global and local scales. On the other hand, electron kinetic effects are also important in the magnetotail thin current sheet [e.g., *Artemyev et al.*, 2016]; a large-scale 3-D particle-in-cell simulation model is needed to fully investigate this scenario with kinetic ions and electrons.

References

Angelopoulos, V., et al. (2008), Tail reconnection triggering substorm onset, *Science*, *321*, 931, doi:10.1126/science.1160495.

Artemyev, A. V., A. A. Petrukovich, R. Nakamura, and L. M. Zelenyi (2011), Cluster statistics of thin current sheets in the Earth magnetotail: Specifics of the dawn flank, proton temperature profiles and electrostatic effects, *J. Geophys. Res.*, *116*, A09233, doi:10.1029/2011JA016801.

Artemyev, A. V., V. Angelopoulos, and A. Runov (2016), On the radial force balance in the quiet-time magnetotail current sheet, *J. Geophys. Res. Space Physics*, *121*, 1017–1026, doi:10.1002/2016JA022180.

Asano, Y., T. Mukai, M. Hoshino, Y. Saito, H. Hayakawa, and T. Nagai (2004), Current sheet structure around the near-Earth neutral line observed by Geotail, *J. Geophys. Res.*, *109*, A02212, doi:10.1029/2003ja010114.

Baker, D. N., T. I. Pulkkinen, V. Angelopoulos, W. Baumjohann, and R. L. McPherron (1996), Neutral line model of substorms: Past results and present view, *J. Geophys. Res.*, *101*(A6), 12,975–13,010, doi:10.1029/95JA03753.

Birmingham, T. J. (1984), Pitch angle diffusion in the Jovian magnetodisc, *J. Geophys. Res.*, *89*(A5), 2699–2707, doi:10.1029/JA089iA05p02699.

Birn, J., et al. (2001), Geospace Environmental Modeling (GEM) magnetic reconnection challenge, *J. Geophys. Res.*, *106*(A3), 3715–3719, doi:10.1029/1999JA900449.

Biskamp, D., and K. Schindler (1971), Instability of two-dimensional collisionless plasma with neutral points, *Plasma Phys.*, *13*, 1013, doi:10.1088/0032-1028/13/11/003.

Borg, A. L., M. Øieroset, T. D. Phan, F. S. Mozer, A. Pedersen, C. Mouikis, J. P. McFadden, C. Twitty, A. Balogh, and H. Rème (2005), Cluster encounter of a magnetic reconnection diffusion region in the near-Earth magnetotail on September 19, 2003, *Geophys. Res. Lett.*, *32*, L19105, doi:10.1029/2005GL023794.

Büchner, J., and L. M. Zelenyi (1986), Deterministic chaos in the dynamics of charged particles near a magnetic field reversal, *Phys. Lett. A*, *118*, 395–399, doi:10.1016/0375-9601(86)90268-9.

Büchner, J., and L. M. Zelenyi (1989), Regular and chaotic charged particle motion in magnetotail-like field reversals: 1. Basic theory of trapped motion, *J. Geophys. Res.*, *94*, 11,821–11,842, doi:10.1029/JA094iA09p11821.

Burkhart, G. R., J. F. Drake, P. B. Dusenbery, and T. W. Speiser (1992), A particle model for magnetotail neutral sheet equilibria, *J. Geophys. Res.*, *97*(A9), 13,799–13,815, doi:10.1029/92JA00495.

Delcourt, D. C., and G. Belmont (1998), Ion dynamics at the earthward termination of the magnetotail current sheet, *J. Geophys. Res.*, *103*(A3), 4605–4613, doi:10.1029/97JA01844.

Eastwood, J. P., T. D. Phan, M. Øieroset, and M. A. Shay (2010), Average properties of the magnetic reconnection ion diffusion region in the Earthʹs magnetotail: The 2001–2005 Cluster observations and comparison with simulations, *J. Geophys. Res.*, *115*, A08215, doi:10.1029/2009ja014962.

Frey, H. U., and S. B. Mende (2006), Substorm onset as observed by IMAGE-FUV, in *Proceedings of the Eighth International Conference on Substorms (ICS-8)*, edited by M. Syrjäsuo and E. Donovan, pp. 71–75 , Univ. of Calgary, Calgary, Alberta, Canada.

Fujimoto, K. (2006), Time evolution of the electron diffusion region and the reconnection rate in fully kinetic and large system, *Phys. Plasmas*, *13*, 072904, doi:10.1063/1.2220534.

Gabrielse, C., V. Angelopoulos, A. Runov, and D. L. Turner (2014), Statistical characteristics of particle injections throughout the equatorial magnetotail, *J. Geophys. Res. Space Physics*, *119*, 2512–2535, doi:10.1002/2013JA019638.

Genestreti, K. J., S. A. Fuselier, J. Goldstein, T. Nagai, and J. P. Eastwood (2014), The location and rate of occurrence of near-Earth magnetotail reconnection as observed by Cluster and Geotail, *J. Atmos. Sol. Terr. Phys.*, *121*, 98–109, doi:10.1016/j.jastp.2014.10.005.

Guild, T. B., H. E. Spence, E. L. Kepko, V. Merkin, J. G. Lyon, M. Wiltberger, and C. C. Goodrich (2008), Geotail and LFM comparisons of plasma sheet climatology: 1. Average values, *J. Geophys. Res.*, *113*, A04216, doi:10.1029/2007JA012611.

Hesse, M., D. Winske, and J. Birn (1998), On the ion-scale structure of thin current sheets in the magnetotail, *Phys. Scr.*, *T74*, 63–66, doi:10.1088/0031-8949/1998/T74/012.

Hesse, M., K. Schindler, J. Birn, and M. Kuznetsova (1999), The diffusion region in collisionless magnetic reconnection, *Phys. Plasmas*, *6*, 1781–1795, doi:10.1063/1.873436.

Hu, Y. Q., X. C. Guo, and C. Wang (2007), On the ionospheric and reconnection potentials of the Earth: Results from global MHD simulations, *J. Geophys. Res.*, *112*, A07215, doi:10.1029/2006JA012145.

Imber, S. M., J. A. Slavin, H. U. Auster, and V. Angelopoulos (2011), A THEMIS survey of flux ropes and traveling compression regions: Location of the near-Earth reconnection site during solar minimum, *J. Geophys. Res.*, *116*, A02201, doi:10.1029/2010ja016026.

Keesee, A. M., N. Buzulukova, J. Goldstein, D. J. Mccomas, E. E. Scime, H. Spence, M. C. Fok, and K. Tallaksen (2011), Remote observations of ion temperatures in the quiet time magnetosphere, *Geophys. Res. Lett.*, *38*, L03104, doi:10.1029/2010GL045987.

Lin, Y., X. Y. Wang, S. Lu, J. D. Perez, and Q. M. Lu (2014), Investigation of storm-time magnetotail and ion injection using three-dimensional global hybrid simulation, *J. Geophys. Res. Space Physics*, *119*, 7413–7432, doi:10.1002/2014JA020005.

Liu, J., V. Angelopoulos, A. Runov, and X.-Z. Zhou (2013), On the current sheets surrounding dipolarizing flux bundles in the magnetotail: The case for wedgelets, *J. Geophys. Res. Space Physics*, *118*, 2000–2020, doi:10.1002/jgra.50092.

Lotko, W., R. H. Smith, B. Z. Zhang, J. E. Ouellette, O. J. Brambles, and J. G. Lyon (2014), Ionospheric control of magnetotail reconnection, *Science*, *345*, 184, doi:10.1126/science.1252907.

Lu, S., Y. Lin, Q. M. Lu, X. Y. Wang, R. S. Wang, C. Huang, M. Y. Wu, and S. Wang (2015a), Evolution of flux ropes in the magnetotail: A three-dimensional global hybrid simulation, *Phys. Plasmas*, *22*, 052901, doi:10.1063/1.4919615.

Lu, S., et al. (2015b), Dipolarization fronts as earthward propagating flux ropes: A three-dimensional global hybrid simulation, *J. Geophys. Res. Space Physics*, *120*, 6286–6300, doi:10.1002/2015JA021213.

Machida, S., Y. Miyashita, A. Ieda, A. Nishida, T. Mukai, Y. Saito, and S. Kokubun (1999), Geotail observations of flow velocity and north-south magnetic field variations in the near and mid-distant tail associated with substorm onsets, *Geophys. Res. Lett.*, *26*(6), 635–638, doi:10.1029/1999GL900030.

Nagai, T., and S. Machida (1998), Magnetic reconnection in the near-Earth magnetotail, in *New Perspectives on the Earthʹs Magnetotail*, *Geophys. Monogr. Ser.*, vol. 105, edited by A. Nishida, D. N. Baker, and S. W. H. Cowley, pp. 211–224 , AGU, Washington, D. C.

Nagai, T., M. Fujimoto, Y. Saito, S. Machida, T. Terasawa, R. Nakamura, T. Yamamoto, T. Mukai, A. Nishida, and S. Kokubun (1998), Structure and dynamics of magnetic reconnection for substorm onset with Geotail observations, *J. Geophys. Res.*, *103*(A3), 4419–4449, doi:10.1029/97JA02190.

Nagai, T., I. Shinohara, M. Fujimoto, M. Hoshino, Y. Saito, S. Machida, and T. Mukai (2001), Geotail observations of the Hall current system: Evidence of magnetic reconnection in the magnetotail, *J. Geophys. Res.*, *106*(A11), 25,929–25,949, doi:10.1029/2001JA900038.

Nagai, T., I. Shinohara, S. Zenitani, R. Nakamura, T. K. M. Nakamura, M. Fujimoto, Y. Saito, and T. Mukai (2013), Three-dimensional structure of magnetic reconnection in the magnetotail from Geotail observations, *J. Geophys. Res. Space Physics*, *118*, 1667–1678, doi:10.1002/jgra.50247.

Petrukovich, A. A., A. V. Artemyev, H. V. Malova, V. Y. Popov, R. Nakamura, and L. M. Zelenyi (2011), Embedded current sheets in the Earthʹs magnetotail, *J. Geophys. Res.*, *116*, A00I25, doi:10.1029/2010JA015749.

Pritchett, P. L., and F. V. Coroniti (1994), Convection and the formation of thin current sheets in the near-Earth plasma sheet, *Geophys. Res. Lett.*, *21*(15), 1587–1590, doi:10.1029/94GL01364.

Pritchett, P. L., and F. V. Coroniti (1995), Formation of thin current sheets during plasma sheet convection, *J. Geophys. Res.*, *100*(A12), 23,551–23,565, doi:10.1029/95JA02540.

Pritchett, P. L., F. V. Coroniti, and V. K. Decyk (1996), Three-dimensional stability of thin quasi-neutral current sheets, *J. Geophys. Res.*, *101*(A12), 27,413–27,429, doi:10.1029/96JA02665.

Raeder, J., R. J. Walker, and M. Ashour-Abdalla (1995), The structure of the distant magnetotail during long periods of northward IMF, *Geophys. Res. Lett.*, *22*, 349–352, doi:10.1029/94GL03380.

Raj, A., T. Phan, R. P. Lin, and V. Angelopoulos (2002), Wind survey of high-speed bulk flows and field-aligned beams in the near-Earth plasma sheet, *J. Geophys. Res.*, *107*(A12), 1419, doi:10.1029/2001ja007547.

Runov, A., et al. (2006), Local structure of the magnetotail current sheet: 2001 Cluster observations, *Ann. Geophys.*, *24*, 247–262, doi:10.5194/angeo-24-247-2006.

Schindler, K., and J. Birn (2002), Models of two-dimensional embedded thin current sheets from Vlasov theory, *J. Geophys. Res.*, *107*(A8), 1193, doi:10.1029/2001JA000304.

Schindler, K., J. Birn, and M. Hesse (2012), Kinetic model of electron potentials in localized collisionless plasma structures under steady quasi-gyrotropic conditions, *Phys. Plasmas*, *19*, 082904, doi:10.1063/1.4747162.

Shay, M. A., J. F. Drake, R. E. Denton, and D. Biskamp (1998), Structure of the dissipation region during collisionless magnetic reconnection, *J. Geophys. Res.*, *103*(A5), 9165–9176, doi:10.1029/97JA03528.

Sitnov, M. I., L. M. Zelenyi, H. V. Malova, and A. S. Sharma (2000), Thin current sheet embedded within a thicker plasma sheet: Self-consistent kinetic theory, *J. Geophys. Res.*, *105*(A6), 13,029–13,043, doi:10.1029/1999JA000431.

Sitnov, M. I., M. Swisdak, P. N. Guzdar, and A. Runov (2006), Structure and dynamics of a new class of thin current sheets, *J. Geophys. Res.*, *111*, A08204, doi:10.1029/2005JA011517.

Slavin, J. A., E. I. Tanskanen, M. Hesse, C. J. Owen, M. W. Dunlop, S. Imber, E. A. Lucek, A. Balogh, and K. H. Glassmeier (2005), Cluster observations of traveling compression regions in the near-tail, *J. Geophys. Res.*, *110*, A06207, doi:10.1029/2004ja010878.

Sonnerup, B. U. O. (1971), Adiabatic particle orbits in a magnetic null sheet, *J. Geophys. Res.*, *76*, 8211–8222, doi:10.1029/JA076i034p08211.

Spence, H. E., and M. G. Kivelson (1990), The variation of the plasma sheet polytropic index along the midnight meridian in a finite width magnetotail, *Geophys. Res. Lett.*, *17*, 591–594, doi:10.1029/GL017i005p00591.

Swift, D. W. (1996), Use of a hybrid code for a global-scale plasma simulation, *J. Comput. Phys.*, *126*, 109, doi:10.1006/jcph.1996.0124.

Vasko, I. Y., A. A. Petrukovich, A. V. Artemyev, R. Nakamura, and L. M. Zelenyi (2015), Earth's distant magnetotail current sheet near and beyond lunar orbit, *J. Geophys. Res. Space Physics*, *120*, 8663–8680, doi:10.1002/2015JA021633.

Walsh, A. P., et al. (2014), Dawn-dusk asymmetries in the coupled solar wind-magnetosphere-ionosphere system: A review, *Ann. Geophys.*, *32*, 705–737, doi:10.5194/angeo-32-705-2014.

Wang, C.-P., L. R. Lyons, J. M. Weyand, T. Nagai, and R. W. McEntire (2006), Equatorial distributions of the plasma sheet ions, their electric and magnetic drifts, and magnetic fields under different interplanetary magnetic field B_z conditions, *J. Geophys. Res.*, *111*, A04215, doi:10.1029/2005JA011545.

Yoon, P. H., and A. T. Y. Lui (2004), Model of ion- or electron-dominated current sheet, *J. Geophys. Res.*, *109*, A11213, doi:10.1029/2004JA010555.

Zelenyi, L. M., M. I. Sitnov, H. V. Malova, and A. S. Sharma (2000), Thin and superthin ion current sheets, quasiadiabatic and nonadiabatic models, *Nonlinear Proc. Geophys.*, *7*, 127–139.

Zelenyi, L. M., A. V. Artemyev, and A. A. Petrukovich (2010), Earthward electric field in the magnetotail: Cluster observations and theoretical estimates, *Geophys. Res. Lett.*, *37*, L06105, doi:10.1029/2009GL042099.

Zhou, X.-Z., et al. (2009), Thin current sheet in the substorm late growth phase: Modeling of THEMIS observations, *J. Geophys. Res.*, *114*, A03223, doi:10.1029/2008JA013777.